45th AIAA Aerospace Sciences Meeting and Exhibit, 8–11 January 2007, Reno NV

Synchronization of Weighted Essentially Non-Oscillatory Methods

Ellen M. Taylor* and M. Pino Martín†
Princeton University, Princeton NJ 08544

Weighted essentially non-oscillatory (WENO) methods have been developed to simultaneously provide robust shock-capturing in compressible fluid flow and avoid excessive damping of fine-scale flow features such as turbulence. Under certain conditions in compressible turbulence, however, numerical dissipation remains unacceptably high even after optimization of the linear component that dominates in smooth regions. We demonstrate that a significant *non*linear source of dissipation error is a "synchronization deficiency" that interferes with the expression of theoretically predicted numerical performance characteristics when the WENO adaptation mechanism is engaged. We furthermore develop and evaluate a technique that meaningfully reduces numerical dissipation associated with the synchronization deficiency but that also faces significant obstacles to practical implementation that currently remain unresolved.

I. Introduction

The detailed simulation of compressible turbulence requires numerical methods that simultaneously avoid excessive damping of spatial features over a large range of length scales and prevent spurious oscillations near shocks and shocklets (small transient shocks) through robust shock-capturing. Numerical schemes that were developed to satisfy these constraints include, among others, weighted essentially non-oscillatory (WENO) methods.[1] WENO schemes compute numerical fluxes using several different candidate stencils and form a final flux approximation by summing weighted contributions from each stencil. Thus they are nonlinear. Smoothness measurements cause stencils that span large flow field gradients to be assigned small relative weights so that a nearly discontinuous shock would provide a weight of almost zero to any stencil containing it. In smooth regions, the relative values of the weights are designed to be optimal by some gauge such as maximum order of accuracy or maximum bandwidth-resolving efficiency.

Jiang and Shu[2] cast the WENO methodology into finite-difference form and provide an efficient implementation of robust and high-order-accurate WENO schemes. Unfortunately, these schemes often generate excessive numerical dissipation for detailed simulations of turbulence, especially for large-eddy simulations (LES).[3] WENO dissipation arises from two distinct sources: (i) the optimal stencil, which by itself describes a linear scheme, and (ii) the adaptation mechanism, which drives the final numerical stencil away from the optimal one. Bandwidth optimization can reduce the dissipation of the optimal stencil;[4,5] and Martín et al.[5] demonstrate that such a bandwidth-optimized symmetric WENO method indeed reduces numerical dissipation and provides accurate results for direct numerical simulations (DNS) of isotropic turbulence and turbulent boundary layers.

Nonetheless, engaging the nonlinear WENO adaptation mechanism still causes significant local dissipation that can negatively affect global flow properties. Though higher resolution compensates for this, in some cases adequately increasing the number of grid points is not feasible. There are two primary sources of nonlinear error: (i) the smoothness measurement that governs the application of WENO stencil adaptation and (ii) the numerical properties of individual candidate stencils that govern numerical accuracy when adaptation engages. Wang and Chen[6] have examined both sources for upwind-biased WENO methods in

*Ph.D. Student and AIAA Member.
†Assistant Professor and AIAA Member.

linearized problems; Ponziani et al.[7] have examined the second source for symmetric WENO methods in linear and nonlinear problems, including isotropic turbulence; and Henrick et al.[8] have examined the first source for upwind-biased WENO methods in linear and nonlinear problems. Additionally, Taylor et al.[9] have examined the first source for symmetric WENO methods in linear and nonlinear problems, including isotropic turbulence, and have introduced a linearly and nonlinearly optimized WENO method that allows accurate DNS of compressible turbulence with significantly reduced grid sizes.[9–11]

The purpose of this paper is to demonstrate that there exists a WENO "synchronization deficiency" that interferes with the expression of theoretically predicted candidate stencil properties and as a result generates excessive numerical dissipation through the second nonlinear error pathway described above. We furthermore develop and evaluate a forced synchronization technique that meaningfully reduces such dissipation but also faces significant obstacles to practical implementation. Section II briefly describes the WENO methodology. In Section III, we introduce the concept of the synchronization deficiency along with numerical evidence of its consequences. Section IV then develops the forced synchronization technique and discusses its benefits and drawbacks. Conclusions are drawn in Section V.

II. WENO Methodology

We describe the symmetric WENO methodology[4,5] in the context of the one-dimensional advection equation,

$$\frac{\partial u}{\partial t} + \frac{\partial}{\partial x} f(u) = 0 \tag{1}$$

This model equation represents the decoupled forms of equations belonging to any system of hyperbolic conservation laws after a transformation from physical into characteristic space. If the spatial domain is discretized such that $x_i = i\Delta$, in which Δ is the grid spacing, and $u_i = u\left(x_i\right)$, Eq. (1) may be cast into the semidiscretized form

$$\frac{du_i}{dt} = -\frac{1}{\Delta}\left(\hat{f}_{i+\frac{1}{2}} - \hat{f}_{i-\frac{1}{2}}\right) \tag{2}$$

in which $\hat{f}_{i+1/2}$ is a numerical approximation of $f\big(u(x_{i+1/2})\big)$. Once the right-hand side of this expression has been evaluated, numerical techniques for solving ordinary differential equations, such as Runge-Kutta methods, may be employed to advance the solution in time. In order to ensure stability, procedures that approximate $f(u)$ split it into $f^+(u)$, which has a strictly non-negative derivative, and $f^-(u)$, which has a strictly non-positive one.

WENO schemes compute $\hat{f}^+_{i+1/2}$ through reconstructed interpolating polynomials on a number of candidate stencils each containing r grid points. In the symmetric WENO method, there are $(r+1)$ stencils in total. The one fully upwinded stencil ranges from $(i-r+1)$ to i, the one fully downwinded stencil ranges from $(i+1)$ to $(i+r)$, and the other stencils fall in between these two extremes. Figure 1 provides a schematic of this arrangement for $r = 3$. Throughout this paper, we will abbreviate any WENO implementation in which the candidate stencils contain r points as "WENO-r."

If the flux approximation on stencil k, which contains r grid points, is designated as q^r_k and the weight assigned to that stencil is ω_k, the final numerical approximation becomes

$$\hat{f}^+_{i+\frac{1}{2}} = \sum_{k=0}^{r} \omega_k q^r_k \tag{3}$$

Specifically, q^r_k emerge from reconstructed polynomial interpolants of maximal order r and are defined as

$$q^r_k \Big|_{i+\frac{1}{2}} = \sum_{l=0}^{r-1} a^r_{kl}\, f(u_{i-r+k+l+1}) \tag{4}$$

in which a^r_{kl} are tabulated coefficients; and ω_k are normalized forms of weights Ω_k defined as

$$\Omega_k = \frac{C^r_k}{(\varepsilon + IS_k)^p} \tag{5}$$

in which ε prevents division by zero, IS_k is a smoothness measurement that becomes large when discontinuities are present within stencil k, and p may be varied to increase or decrease WENO adaptation sensitivity. $p = 1$ typically provides sufficient adaptation with minimal dissipation. In completely smooth regions, each stencil is equally desirable, and ω_k revert to the optimal weights C_k.

The corresponding stencil diagram for $\hat{f}^{-}_{i+1/2}$ is simply a mirror image of Fig. 1. Because the total number of data points available to the symmetric WENO algorithm is $2r$, its maximum order of accuracy is also $2r$; however, the optimal stencils employed in the current work are bandwidth-optimized[4,5] such that only rth-order accuracy can be guaranteed. The bandwidth-optimization process also introduces a small amount of artificial dissipation to an otherwise neutrally stable optimal stencil to enhance its stability. In practice, the weight of the fully downwinded stencil ω_r is artificially constrained to be no greater than the least of the others so that other adverse stability effects are avoided.

The continuity of the WENO weighting process allows the performance characteristics of the final numerical stencil to theoretically fall anywhere between those of the least favorable candidate stencil and those of the optimal stencil. In order to gauge this variation quantitatively but efficiently in a flow field, Weirs[4] proposed a combination of the adaptive stencil weights called the nonlinearity index (NI). It is essentially a measure of the degree of departure from the optimal stencil and is defined as

$$NI = \left(\sum_{k=0}^{r} \left[1 - \frac{(r+1)\,(\Omega_k / C_k)}{\sum_{l=0}^{r} (\Omega_l / C_l)} \right]^2 \right)^{\frac{1}{2}} \tag{6}$$

This definition forces NI to always be non-negative, and only the optimal stencil can provide a value of zero. It reaches its theoretical maximum, which is $\sqrt{r\,(r+1)}$, when any one candidate stencil is chosen exclusively. We will often report NI in terms of NI', its value normalized by this maximum.

III. Synchronization Deficiency

A. Theory

In theory, the numerical performance characteristics (e.g. bandwidth-resolving capabilities) of the least favorable WENO candidate stencil dictate a definitive lower bound on the performance characteristics of any possible final weighted numerical stencil. If the flux approximation $\hat{f}_{i+1/2}$, calculated according to the previous section, encompassed the entirety of the flux information required to approximate a spatial derivative, this would be true in practice as well. Of course, in addition to $\hat{f}_{i+1/2}$, Eq. (2) demands $\hat{f}_{i-1/2}$, which is rarely explicitly acknowledged because its calculation consists merely of shifting an index. Its presence, however, significantly complicates the question of performance characteristics.

Let us fully expand Eq. (2), the left-hand side of which depends on a fixed combination of $\hat{f}_{i+1/2}$ and $\hat{f}_{i-1/2}$. According to Eqs. (3) and (4),

$$\hat{f}_{i+\frac{1}{2}} = \sum_{k=0}^{r} \omega_k \sum_{l=0}^{r-1} a^r_{kl}\, f_{i-r+k+l+1} \tag{7a}$$

$$\hat{f}_{i-\frac{1}{2}} = \sum_{k=0}^{r} \omega_k \sum_{l=0}^{r-1} a^r_{kl}\, f_{i-r+k+l} \tag{7b}$$

and so

$$\begin{aligned} \frac{du_i}{dt} &= -\frac{1}{\Delta} \left(\hat{f}_{i+\frac{1}{2}} - \hat{f}_{i-\frac{1}{2}} \right) \\ &= -\frac{1}{\Delta} \sum_{k=0}^{r} \omega_k \left[a^r_{k,r-1}\, f_{i+k} - a^r_{k,0}\, f_{i-r+k} + \sum_{l=1}^{r-1} \left(a^r_{k,l-1} - a^r_{kl} \right) f_{i-r+k+l} \right] \\ &= -\frac{1}{\Delta} \sum_{k=0}^{r} \omega_k \sum_{l=0}^{r} b^r_{kl}\, f_{i-r+k+l} \end{aligned} \tag{8}$$

in which coefficients can be equated to yield

$$b_{kl}^r = \begin{cases} -a_{k,0}^r, & l = 0 \\ a_{k,l-1}^r - a_{kl}^r, & 0 < l < r \\ a_{k,r-1}^r, & l = r \end{cases} \tag{9}$$

The coefficients b_{kl}^r, rather than a_{kl}^r, are the relevant parameters for determining and optimizing the properties of the kth candidate stencil. Since b_{kl}^r are independent of the adaptive quantities ω_k, the performance characteristics of individual candidates appear to be guaranteed regardless of local WENO adaptation. The flaw in this argument is the implicit assumption in Eq. (7) that ω_k are equal for $\hat{f}_{i+1/2}$ and $\hat{f}_{i-1/2}$.

The smoothness measurement IS_k depends entirely on the flux information available within stencil k, which spans different points for $\hat{f}_{i+1/2}$ and $\hat{f}_{i-1/2}$. Because the collections of data values on the two versions of the stencil will in general be unequal, the associated stencil weights ω_k must be assumed to vary. If we define $\omega_k^\pm$ to mean the ω_k that belong to $\hat{f}_{i\pm1/2}$, Eq. (7) becomes

$$\hat{f}_{i+\frac{1}{2}} = \sum_{k=0}^{r} \omega_k^+ \sum_{l=0}^{r-1} a_{kl}^r \, f_{i-r+k+l+1} \tag{10a}$$

$$\hat{f}_{i-\frac{1}{2}} = \sum_{k=0}^{r} \omega_k^- \sum_{l=0}^{r-1} a_{kl}^r \, f_{i-r+k+l} \tag{10b}$$

and in turn Eq. (8) becomes

$$\begin{aligned} \frac{du_i}{dt} &= -\frac{1}{\Delta}\left(\hat{f}_{i+\frac{1}{2}} - \hat{f}_{i-\frac{1}{2}}\right) \\ &= -\frac{1}{\Delta}\sum_{k=0}^{r} \omega_k^+ \left[a_{k,r-1}^r \, f_{i+k} - \frac{\omega_k^-}{\omega_k^+} a_{k,0}^r \, f_{i-r+k} + \sum_{l=1}^{r-1} \left(a_{k,l-1}^r - \frac{\omega_k^-}{\omega_k^+} a_{kl}^r \right) f_{i-r+k+l} \right] \\ &= -\frac{1}{\Delta}\sum_{k=0}^{r} \omega_k^+ \sum_{l=0}^{r} \widetilde{b_{kl}^r} \, f_{i-r+k+l} \end{aligned} \tag{11}$$

in which coefficients can be equated to yield

$$\widetilde{b_{kl}^r} = \begin{cases} -\frac{\omega_k^-}{\omega_k^+} a_{k,0}^r, & l = 0 \\ a_{k,l-1}^r - \frac{\omega_k^-}{\omega_k^+} a_{kl}^r, & 0 < l < r \\ a_{k,r-1}^r, & l = r \end{cases} \tag{12}$$

The relevant parameters for determining and optimizing the properties of the kth candidate stencil are now the new coefficients $\widetilde{b_{kl}^r}$. These, unlike the old b_{kl}^r, do depend on the adaptive quantities $\omega_k^\pm$; and, since a_{kl}^r are fixed, $\widetilde{b_{kl}^r} = b_{kl}^r$ if and only if $\omega_k^- = \omega_k^+$. Note that equality necessarily holds when $\hat{f}_{i\pm1/2}$ both employ the optimal stencil weights C_k^r. In regions in which WENO adaptation has engaged, however, inequality can force the actual individual stencil characteristics to diverge from the expected theoretical properties described by b_{kl}^r.

The theoretical error characteristics of a finite-difference scheme are often quantitatively presented in the form of a modified wavenumber plot. Consider a linearly convected pure harmonic function of the form

$$f(x) = e^{ikx} = e^{i\kappa x/\Delta} \tag{13}$$

in which x is position, Δ is grid spacing, and k and κ are dimensional and nondimensional wavenumbers, respectively. The finite-difference approximation to its spatial derivative is equivalent to the analytic derivative of a similarly defined function with the modified wavenumber

$$\kappa'(\kappa) = -i \sum_n c_n \, e^{in\kappa} \tag{14}$$

in which the coefficients c_n specify the numerical scheme employed. The real and imaginary parts of κ' describe phase and amplitude properties, respectively, and a hypothetical finite-difference scheme that fully resolved all wavenumbers would produce $\kappa' = \kappa$ for $0 \le \kappa \le \pi$. In the present case of symmetric WENO methods,

$$c_n = \begin{cases} -\omega_0^- a_{0,0}^r, & n = -r \\ \displaystyle\sum_{m=0}^{r+n-1} \omega_m^+ a_{m,r+n-m-1}^r - \sum_{m=0}^{r+n} \omega_m^- a_{m,r+n-m}^r, & -r < n < 0 \\ \displaystyle\sum_{m=0}^{r-1} \omega_m^+ a_{m,r-m-1}^r - \sum_{m=1}^{r} \omega_m^- a_{m,r-m}^r, & n = 0 \\ \displaystyle\sum_{m=n}^{r} \omega_m^+ a_{m,r+n-m-1}^r - \sum_{m=n+1}^{r} \omega_m^- a_{m,r+n-m}^r, & 0 < n < r \\ \omega_r^+ a_{r,r-1}^r, & n = r \end{cases} \tag{15}$$

In Fig. 2, we display the theoretical bandwidth properties of the linearly optimized WENO-3 scheme[4,5] for an illustrative possible scenario in which the stencil weights are such that, for the calculation $\hat{f}_{i-1/2}$ ("left-hand" calculation), the first *three* stencils are equally utilized and the last one discarded, and for the calculation of $\hat{f}_{i+1/2}$ ("right-hand" calculation), the first *two* stencils are equally utilized and the last two discarded. Figure 1 provides a useful graphical reference for visualizing this scenario. Since the left-hand arrangement incorporates more grid points and is more centrally situated relative to the point of interest, we would expect its numerical characteristics to be more favorable than those of the right-hand arrangement. Indeed, Fig. 2(a) confirms that if both calculations were forced to use the left-hand arrangement ("synchronized left") rather than the right-hand one ("synchronized right"), the modified wavenumber would more closely approximate the exact wavenumber. It also shows that when the calculations are left unsynchronized, the amplitude characteristics are little better than those of the worst component, and the phase characteristics are actually significantly poorer than those of the worst component. The variation in phase characteristics can be seen more clearly in Fig. 2(b), which plots the phase error $\varepsilon = \kappa'/\kappa - 1$.

B. Numerical Evidence

Though the WENO synchronization deficiency is certainly valid from a mathematical standpoint, and even though it can under certain circumstances significantly degrade theoretical bandwidth properties, its cumulative effects on actual numerical simulations may still turn out to be relatively small. We investigate this possibility by implementing a naive forcibly synchronized WENO (SWENO) method for the one-dimensional advection equation of Eq. (1). After obtaining the normalized stencil weights ω_k according to Section II, we set

$$\langle \Omega_k \rangle = \frac{1}{2} \left(\omega_k^+ + \omega_k^- \right) \tag{16}$$

and then normalize $\langle \Omega_k \rangle$ to form the synchronized stencil weights $\langle \omega_k \rangle$ that apply to calculations of both $\hat{f}_{i+1/2}$ and $\hat{f}_{i-1/2}$.

The effects of synchronizing the linearly optimized WENO-4 scheme[4,5] in this manner are presented in Fig. 3, which depicts a linearly advected sine wave with seven points per wavelength after time integration via a third-order-accurate Runge-Kutta scheme for twenty wavelength-times. For reference we include results from the original (unsynchronized) WENO-4 scheme both with and without stencil adaptation permitted. Figure 3(a) shows that, while the WENO-4 scheme causes notable dissipation, the SWENO-4 scheme maintains the proper wave shape nearly as faithfully as when adaptation is completely prohibited. In Fig. 3(b), we plot the nonlinearity index NI' for each of these schemes to demonstrate that the improvement offered by the SWENO method is not due simply to closer conformance to the optimal stencil. The decrease in overall NI' from the adaptation-permitted WENO-4 scheme to the adaptation-prohibited scheme far exceeds the decrease from the former to the SWENO-4 scheme, yet the SWENO-4 flow solution is almost equivalent to the adaptation-prohibited solution.

This exercise proves that the synchronization deficiency is not merely a mathematical curiosity; its consequences unquestionably contaminate the results of numerical simulations.

IV. Forced Synchronization

Attempting to extend the forcibly synchronized WENO method of Section III(B) to non-smooth initial data explains our previous warning that this approach is naive. Consider a linearly advected perfect shock located somewhere between points x_{i-1} and x_i as sketched for $r = 3$ in Fig. 4. Without explicitly calculating the smoothness measurements IS_k and resulting weights ω_k, we can still qualitatively determine that a candidate stencil receives small weight if it crosses the discontinuity and large weight otherwise. Also, recall that the fully downwinded stencil is never allowed to hold more weight than the least-weighted of the others. According to these principles, the bold stencils in the lower portion of Fig. 4 are those independently favored for calculating $\hat{f}_{i\pm1/2}$, and the two resulting stencil arrangements are clearly mutually exclusive. If $\omega_k^{\pm}$ are to be synchronized, some form of compromise is necessary; and any form of compromise under these circumstances will undermine the WENO shock-capturing mechanism.

In order to preserve the robust shock-capturing capability of unsynchronized WENO methods, we must selectively suspend synchronization in immediate neighborhoods (i.e. within approximately one grid spacing) of strong discontinuities. One possible form for a quantitative suspension criterion arises from the root cause of the perfect-shock synchronization failure above, which is the mutual exclusivity of the candidate stencil arrangements favored for computing $\hat{f}_{i\pm1/2}$. In mathematical terms, for the scenario depicted in Fig. 4, the ratio

$$\chi_k = \frac{\min\left(\omega_k^+, \omega_k^-\right)}{\max\left(\omega_k^+, \omega_k^-\right)} \tag{17}$$

is much less than unity for *all* values of k for which ω_k^+ and ω_k^- are not both negligible. In practical terms, this translates to the requirement that forced synchronization must be suspended when

$$\chi_k < \beta \tag{18}$$

in which β is a free parameter, and also that synchronization must be suspended when this holds for *any* candidate stencil rather than for all of them. We will discuss the motivation and implications of the last restriction later in this section; for now, the forcibly synchronized WENO method is complete enough that we may briefly examine the importance of the synchronization deficiency in an example of non-smooth flow.

A. Shu-Osher Problem

The Shu-Osher problem places smooth density fluctuations upstream of a moving shock front to probe the ability of a shock-capturing method to resolve discontinuities embedded within pseudoturbulence without damaging fine structures. In our simulations, the conditions at the right boundary are atmospheric with zero velocity, and the conditions at the left boundary are such that the shock between the two states has a relative incoming Mach number of three. Sinusoidal density fluctuations are imposed upstream of this shock with wavelength $\lambda = \frac{1}{8}L$ and excursions of $\pm 0.2\rho_R$, in which the subscript R indicates the right boundary. Initially, the shock is positioned at $x/L = \lambda$, and we evolve simulations in time via a third-order-accurate Runge-Kutta scheme until $t = 0.21\, L/a_R$. For reference, Fig. 5 displays converged density profiles for the initial and developed states as computed by the WENO-4 scheme on an excessively fine grid of 2048 points. Upon termination, an undisturbed portion of the original fluctuation field lies upstream of the main shock, immediately downstream is a region of physically correct high-frequency fluctuations, and further downstream is a region of low-frequency fluctuations with interspersed shocklets.

In Fig. 6, we examine the effects of forced synchronization, in which we set $\beta = 0.05$ in Eq. (18), on solutions to the Shu-Osher problem as computed by WENO-3 schemes on 192 grid points. Figure 6(a) shows that, at this resolution, the density profile of the original unsynchronized WENO scheme is sufficiently accurate everywhere except within the high-frequency region, where it performs rather poorly. The SWENO scheme, on the other hand, captures these fluctuations visibly more faithfully, indicating that in this case the synchronization deficiency accounts for a large fraction of the excessive dissipation generated by the original WENO method. Profiles of nonlinearity index NI' are presented in Fig. 6(b), and their rough equivalence between the WENO and SWENO schemes indicates that, as we observed in the previous case of the linearly advected sine wave, the benefits of forced synchronization cannot be attributed simply to closer conformance to the optimal stencil.

A similar analysis of synchronized versus unsynchronized WENO-4 schemes yields results that are materially identical to the those presented for the WENO-3 schemes.

B. Obstacles to Practical Implementation

Although the forcibly synchronized WENO method that we have constructed succeeds at reducing excessive dissipation without compromising shock-capturing capability, we find that the practicality of its current form is limited due to several interrelated obstacles.

The first is that an SWENO scheme with r points per candidate stencil demands significantly more computational time than an unsynchronized WENO scheme with the same number of points. Efficient WENO implementations recognize that $\hat{f}_{i+1/2}$ at grid point $i = j$ is equivalent to $\hat{f}_{i-1/2}$ at point $(i = j + 1)$ and therefore calculate only $\hat{f}_{i+1/2}$ at each point. Synchronization, however, introduces the possibility that $\hat{f}_{i+1/2}$ at $i = j$ may depend on different stencil weights than those producing $\hat{f}_{i-1/2}$ at $i = j + 1$; thus SWENO methods must calculate *both* $\hat{f}_{i\pm1/2}$ at every grid point.

The second obstacle is the requirement, for which we have not yet provided full motivation, that forced synchronization must be suspended if Eq. (18) holds for *any* candidate stencil. In other words, synchronization is permitted only if *no* stencil weight is wildly out of synch with its counterpart. If all stencil weight pairs $\omega_k^{\pm}$ are more or less in synch, then no discontinuity is located within the reach of the optimal stencil, and therefore the optimal stencil, which by definition has the most favorable performance characteristics possible, will generate adequately non-oscillatory flux approximations. In previous work,[9] we have constructed and evaluated a modified WENO method that encourages aggressive application of the optimal stencil wherever possible with little increase in computational cost. Since synchronization currently takes place only when the optimal stencil is also appropriate, and since it adds significant computational cost, practicality favors alternative modifications such as the one just described.

During the discussion leading to Eq. (18), we first noted that forced synchronization must be suspended if this equation holds for *all* candidate stencils for which at least one of the stencil weight pair $\omega_k^{\pm}$ is non-negligible; then we shifted without explanation to the more conservative requirement that synchronization must be suspended if it holds for even one stencil. The former criterion, unlike the latter, would allow forced synchronization to proceed even in the vicinity of a discontinuity provided that it was located near the edges of the optimal stencil and not the center. As long as there existed at least one candidate stencil favored by the calculations of both $\hat{f}_{i\pm1/2}$, synchronization would be permitted and its benefits realized. In principle this hypothetical SWENO scheme could accomplish more than is possible by aggressively applying the optimal stencil, but what prevents us from implementing this theoretically superior method is a third, more subtle, obstacle.

The form of the spatial derivative in Eq. (2) is not simply a matter of notational convenience. In the immediate vicinity of a shock, the flux leaving cell $i = j$ to the right ($\hat{f}_{i+1/2}$=$\hat{f}_{j+1/2}$) must precisely equal the flux entering cell $i = j + 1$ from the left ($\hat{f}_{i-1/2}$=$\hat{f}_{j+1/2}$); otherwise, propagation of the shock front proceeds incorrectly. The form of Eq. (2), coupled with the understanding that only $\hat{f}_{i+1/2}$ is explicitly computed at each grid point, guarantees this proper flux behavior. As the point of interest moves away from the shock, the strictly conservative structure may be greatly relaxed, which is why finite-difference constructions that violate this principle, such as central Padé schemes,[12] may be employed without consequence in smooth flow regions. The third obstacle to implementing forced synchronization is that the WENO smoothness measurement technique, as currently formulated, cannot be trusted to identify with sufficient fidelity the non-smooth regions in which precise flux conservation is necessary. As an illustration, in Fig. 7 we plot the profiles of WENO-3 and WENO-4 nonlinearity index NI' that arise from a linearly advected shock wave with a numerical width between three and four grid spacings, which is typical of a well-captured shock. Immediately downstream and upstream of the shock front, high NI' indicates a sufficient impediment to inappropriate synchronization, but within the shock front, where strict flux conservation is paramount, NI' drops dangerously low.

V. Conclusions

When adaptation draws the final numerical stencil away from the optimal stencil, WENO methods exhibit a synchronization deficiency that interferes with the expression of theoretically predicted numerical

performance characteristics, and this contributes significantly to numerical dissipation. We have demonstrated the extent to which forced synchronization can reduce this dissipation in linear advection simulations of smooth oscillations and Euler simulations of the shock/pseudoturbulence interaction of the Shu-Osher problem. Based on these findings, we expect the synchronization deficiency to account for a large fraction of excessive dissipation in general compressible turbulent flows.

Forced synchronization cannot be applied in the immediate vicinity (i.e. within approximately one grid spacing) of a discontinuity because to do so would undermine the shock-capturing capability of the WENO methodology. This constraint is dictated by theoretical and mathematical considerations and is inviolable, but a discontinuity located toward the edges of the optimal stencil can be considered outside the immediate vicinity and is therefore not a necessary condition for synchronization suspension. Unfortunately, the existing WENO smoothness measurement technique poorly distinguishes between non-smooth regions that require a strictly conservative flux-differencing structure and those that do not. Thus, in order to guarantee proper shock propagation, the window in which synchronization can be permitted must be so narrow that similar benefits can be achieved by the computationally simpler procedure of more aggressive application of the optimal stencil.

Because the numerical characteristics of individual candidate stencils are significantly compromised by the WENO synchronization deficiency, we recommend against attempting to improve WENO performance by optimizing candidate stencil coefficients. Any gains produced by such an approach should be negligible. The WENO smoothness measurement technique, on the other hand, has become an even more attractive target than before. If the smoothness measurement could be made to more faithfully identify shock-associated regions, then in addition to any direct benefits to unsynchronized WENO schemes, the expanded opportunities for forced synchronization might render its cost acceptable.

Acknowledgments

This work was sponsored by the National Science Foundation under Grant CTS-0238390. Computational resources were provided by the CRoCCo Laboratory at Princeton University.

References

[1]Liu, X.-D., Osher, S., and Chan, T., "Weighted Essentially Non-Oscillatory Schemes," *Journal of Computational Physics*, Vol. 115, No. 1, 1994, pp. 200–12.

[2]Jiang, G.-S. and Shu, C.-W., "Efficient Implementation of Weighted ENO Schemes," *Journal of Computational Physics*, Vol. 126, No. 1, 1996, pp. 202–28.

[3]Garnier, E., Mossi, M., Sagaut, P., Comte, P., and Deville, M., "On the Use of Shock-Capturing Schemes for Large-Eddy Simulations," *Journal of Computational Physics*, Vol. 153, No. 1, 1999, pp. 273–311.

[4]Weirs, V. G., *A Numerical Method for the Direct Simulation of Compressible Turbulence*, Ph.D. thesis, University of Minnesota, December 1998.

[5]Martín, M. P., Taylor, E. M., Wu, M., and Weirs, V. G., "A Bandwidth-Optimized WENO Scheme for the Effective Direct Numerical Simulation of Compressible Turbulence," *Journal of Computational Physics*, Vol. 220, No. 1, 2006, pp. 270–89.

[6]Wang, Z. J. and Chen, R. F., "Optimized Weighted Essentially Nonoscillatory Schemes for Linear Waves with Discontinuity," *Journal of Computational Physics*, Vol. 174, No. 1, 2001, pp. 381–404.

[7]Ponziani, D., Pirozzoli, S., and Grasso, F., "Development of Optimized Weighted-ENO Schemes for Multiscale Compressible Flows," *International Journal for Numerical Methods in Fluids*, Vol. 42, No. 9, 2003, pp. 953–77.

[8]Henrick, A. K., Aslam, T. D., and Powers, J. M., "Mapped Weighted Essentially Non-Oscillatory Schemes: Achieving Optimal Order Near Critical Points," *Journal of Computational Physics*, Vol. 207, No. 2, 2005, pp. 542–67.

[9]Taylor, E. M., Wu, M., and Martín, M. P., "Optimization of Nonlinear Error for Weighted Essentially Non-Oscillatory Methods in Direct Numerical Simulations of Compressible Turbulence," Journal of Computational Physics in press.

[10]Wu, M. and Martín, M. P., "New DNS Results of Shockwave/Turbulent Boundary Layer Interaction," Paper 2006–3037, American Institute of Aeronautics and Astronautics, 2006.

[11]Wu, M. and Martín, M. P., "Direct Numerical Simulation of Shockwave and Turbulent Boundary Layer Interaction Induced by a Compression Ramp," submitted to AIAA Journal.

[12]Lele, S. K., "Compact Finite-Difference Schemes with Spectral-Like Resolution," *Journal of Computational Physics*, Vol. 103, No. 1, 1992, pp. 16–42.

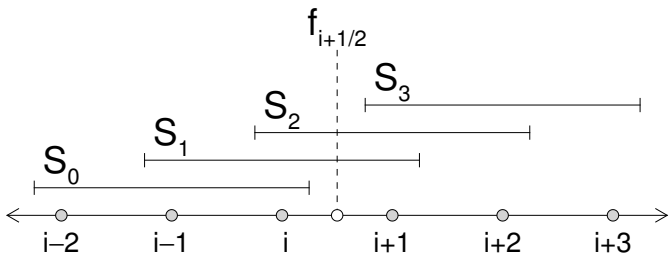

Figure 1. Symmetric WENO candidate stencils for approximating the numerical flux $\hat{f}^{+}_{i+1/2}$ when the number of points per candidate stencil is $r = 3$.

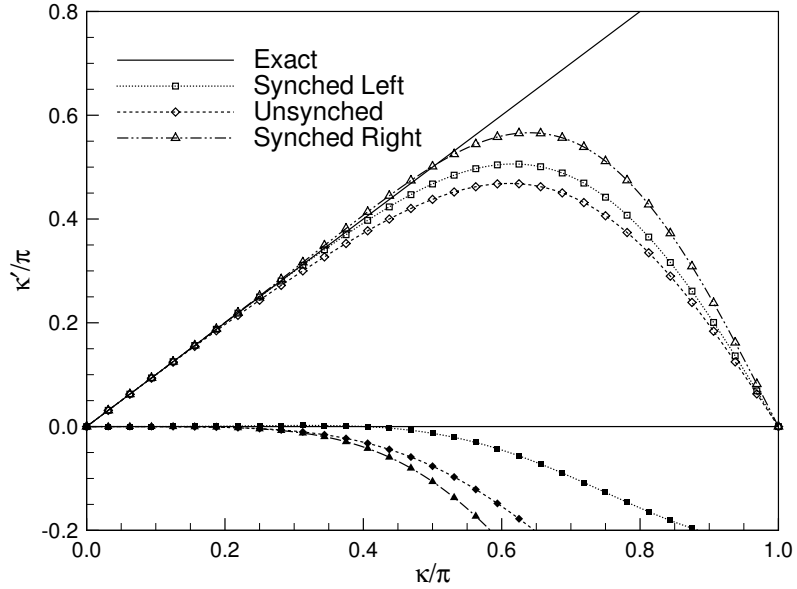

(a) Phase and amplitude representations of the modified wavenumber.

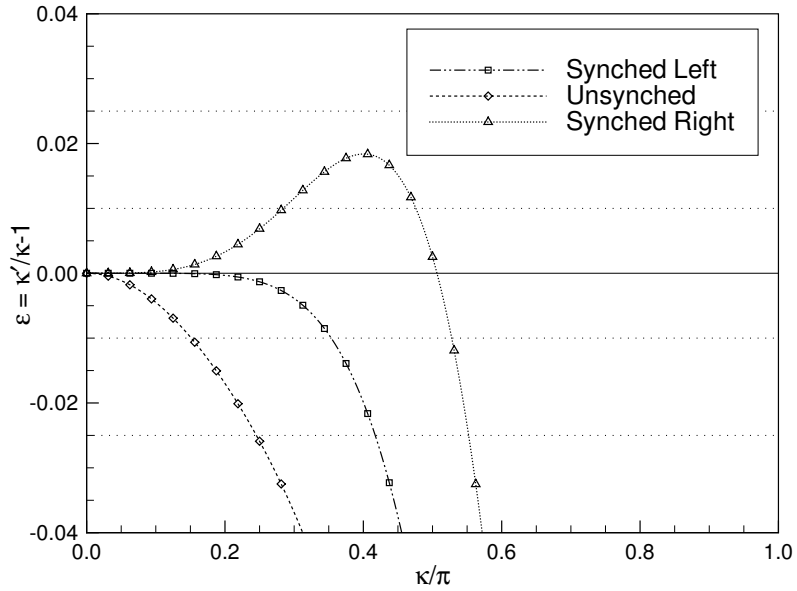

(b) Phase error representation of the modified wavenumber.

Figure 2. Bandwidth properties of the WENO-3 scheme when the "left-hand" calculation utilizes only the first three candidate stencils equally, discarding the last one, and the "right-hand" calculation utilizes only the first two equally, discarding the last two. Open and filled symbols indicate phase and amplitude characteristics, respectively.

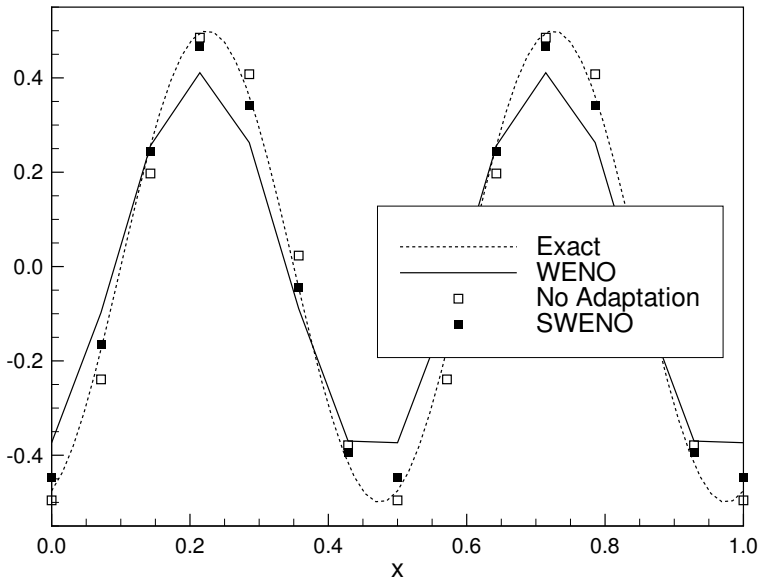

(a) Numerical and exact solutions.

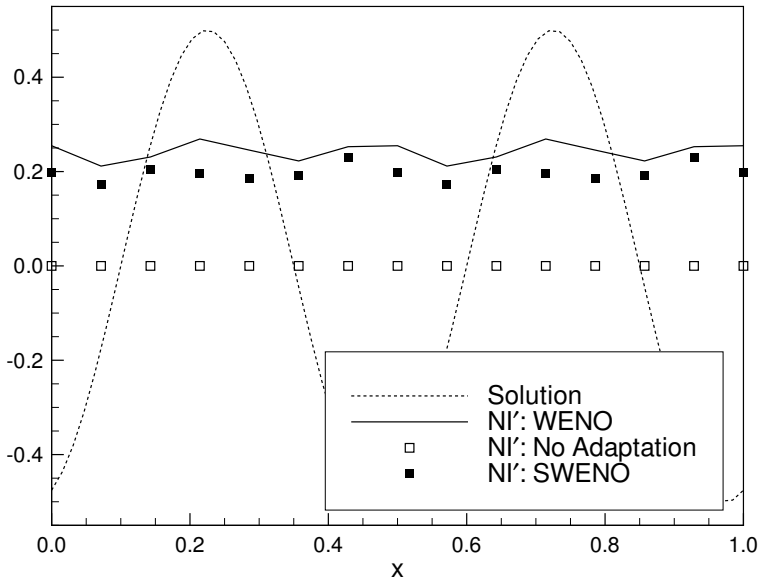

(b) Nonlinearity index NI' layed over the exact solution.

Figure 3. Linearly advected sine wave with seven points per wavelength as computed by WENO-4 and synchronized WENO-4 (SWENO-4) schemes, with and without adaptation, after twenty wavelength-times.

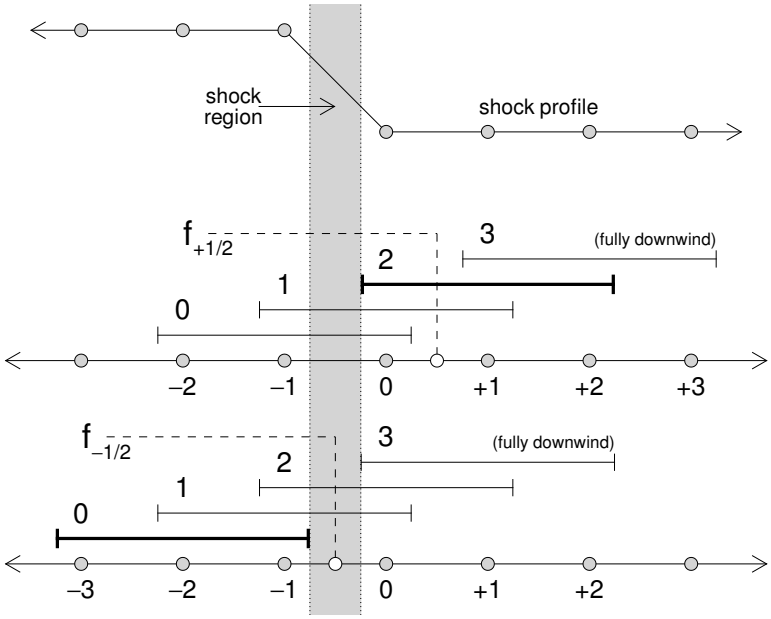

Figure 4. Symmetric WENO candidate stencils for approximating the numerical fluxes $\hat{f}^{+}_{i\pm1/2}$ when the number of points per candidate stencil is $r = 3$ and a perfect shock is located somewhere between points x_{i-1} and x_i. Bold stencils are strongly weighted.

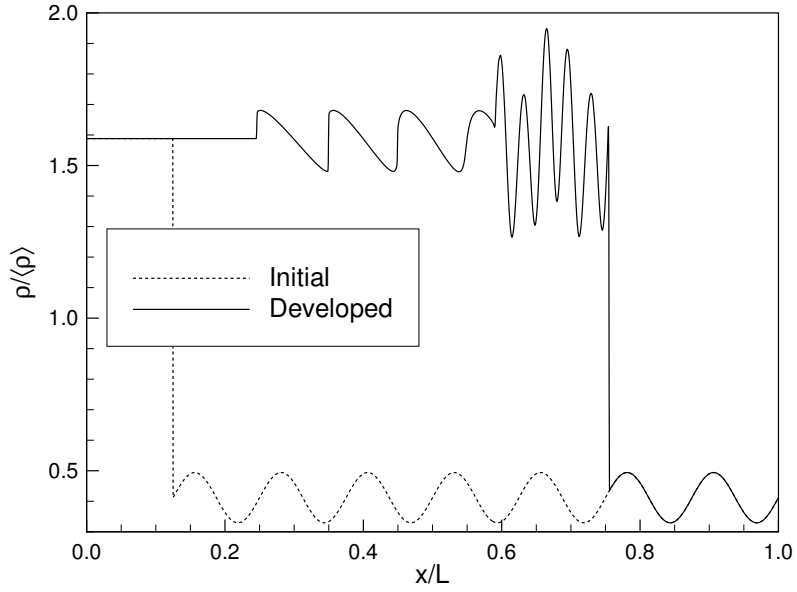

Figure 5. Converged density profiles of the Shu-Osher problem as computed on 2048 grid points by the WENO-4 scheme.

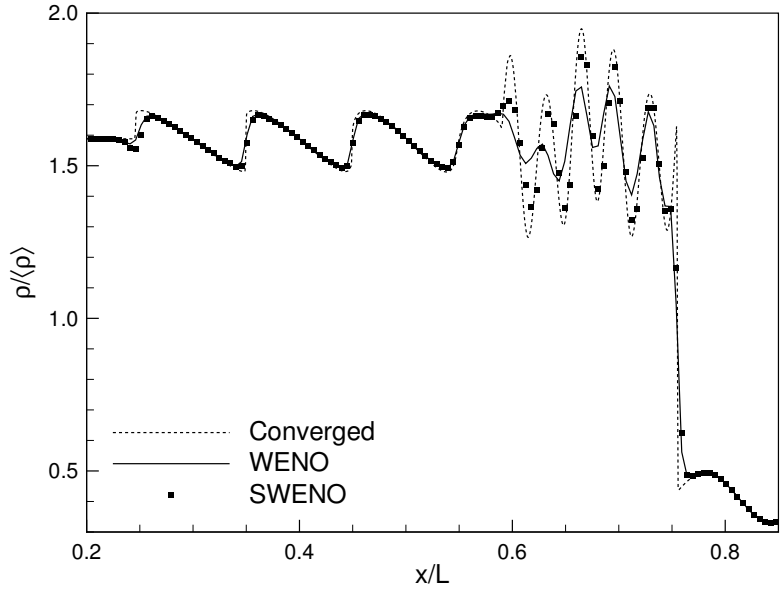

(a) Density profiles.

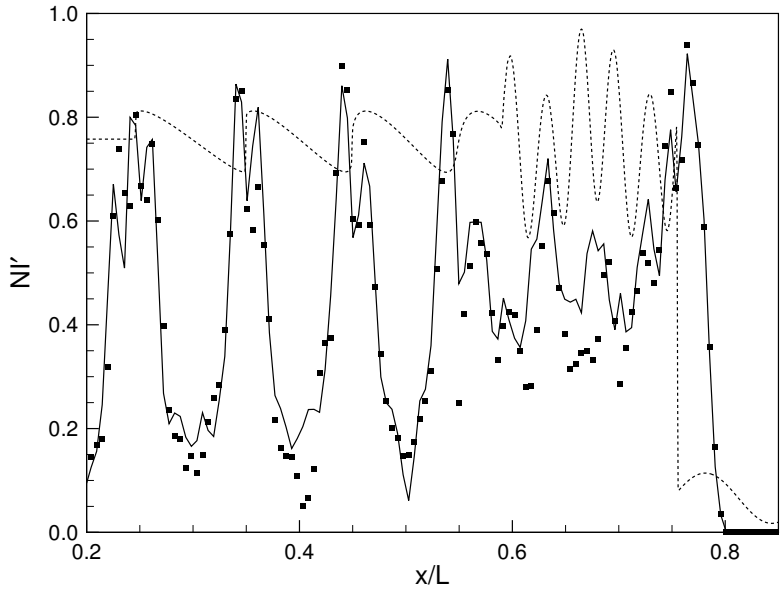

(b) Profiles of nonlinearity index NI'.

Figure 6. Shu-Osher problem as computed on 192 grid points by WENO-3 and synchronized WENO-3 (SWENO-3) schemes.

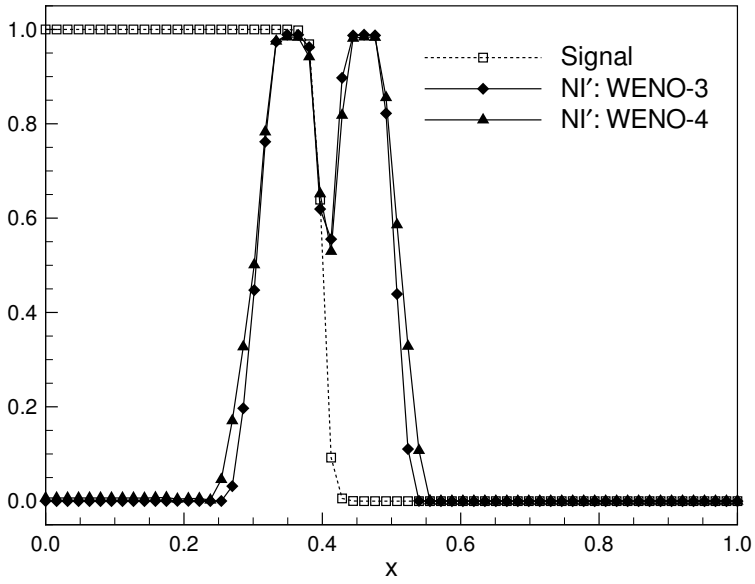

Figure 7. Profiles of WENO-3 and WENO-4 nonlinearity index NI' across a linearly advected shock wave with a numerical width between three and four grid points.